Acta Cryst. (1999). B**55**, 712–720

Structure of and electron density in $RbTiOAsO_4$ at 9.6 K

Jenni Almgren,[a]* Victor A. Streltsov,[b] Alexander N. Sobolev,[c] Brian N. Figgis[c] and Jörgen Albertsson[a]

[a]*Inorganic Chemistry, Chalmers University of Technology, SE-412 96 Göteborg, Sweden,* [b]*Crystallography Centre, University of Western Australia, Nedlands 6907, Australia, and* [c]*Department of Chemistry, University of Western Australia, Nedlands 6907, Australia. E-mail: jean@inoc.chalmers.se*

(*Received 23 December 1998; accepted 9 March 1999*)

Abstract

Structure factors for rubidium titanyl arsenate, $RbTiOAsO_4$, were measured with Mo $K\alpha$ radiation ($\lambda = 0.71069$ Å) at 9.6 and 295 K. The data show that there is no phase transition between room temperature and 9.6 K. The space group is $Pna2_1$. Unit-cell parameters are $a = 13.218$ (1), $b = 6.6500$ (9) and $c = 10.761$ (1) Å at 9.6 K, and $a = 13.261$ (2), $b = 6.6791$ (8) and $c = 10.769$ (1) Å at 295 K. As the temperature was lowered from 295 to 9.6 K the Rb atoms moved along the c axis in the direction of the polarization vector, while no significant change was noted for the Ti–O–As network. Strong accumulation and polarization of the difference electron density ($\Delta\rho$) in exceptionally short covalent Ti—O bonds alternates with the depleted density in long Ti—O bonds. The $\Delta\rho$ near the Ti atoms is polarized and aligned in the negative c direction in accordance with the ferroelectric properties of this material. However, the electron density near the Rb atoms is depleted in this direction and the excess $\Delta\rho$ is moved further away from the nuclei along the c vector.

1. Introduction

Rubidium titanyl arsenate (RTA) is a member of the potassium titanyl phosphate (KTP) family comprising the isostructural MTiOXO$_4$-type compounds. The KTP structure was first solved by Tordjman *et al.* (1974), and since then numerous isomorphs have been studied (Stucky *et al.*, 1989). Some of these crystals are well known for their ferroelectric and nonlinear optical properties, which make them attractive to the electro-optical industry. The KTP isomorphs have an orthorhombic $Pna2_1$ noncentrosymmetric structure consisting of a network of PO_4 tetrahedra and distorted TiO_6 octahedra with PO_4–TiO_6–PO_4–TiO_6 chains along the [100], [010] and [101] directions. The Ti atoms are displaced from their ideal positions in the TiO_6 octahedra forming long and short Ti—O bonds, which are thought to contribute to the nonlinear electro-optical effects. The structural network has channels along the c axis containing two different K sites. Because the K^+ cations can move easily in these channels, the KTP structure has rather high ionic conductivity in the direction of the polar c axis. In contrast, because of the different cation and channel sizes, the RTA structure exhibits much lower ionic conductivity than KTP. This enables the periodic poling of flux-grown RTA crystals (Karlsson *et al.*, 1996; Hu *et al.*, 1996; Risk & Loiacono, 1996). Moreover, owing to higher transmission in the IR region the arsenate analogues can significantly extend the optical range of lasers, making them more versatile (Mangin *et al.*, 1989).

The ferroelectric phase transition in the KTP family of compounds is recognized as a continuous second-order transition, of both displacive and order–disorder type (*e.g.* Belokoneva *et al.*, 1997). The phase-transition temperature T_c is 1207 K for KTP (Stefanovich *et al.*, 1996). The high-temperature paraelectric *Pnan* centrosymmetric structure was determined by single-crystal neutron diffraction for $TlTiOPO_4$ (Harrison *et al.*, 1990) and by single-crystal X-ray diffraction for $TlSbOGeO_4$ (Belokoneva *et al.*, 1993). At $T > T_c$ the number of the O-atom sites is halved, the Ti and P atoms move to special positions, and the alkali-metal atoms occupy split sites. During the transformation from the paraelectric to the ferroelectric phase, the alkali-metal ions are significantly displaced along the polarization vector, falling into two independent sites. This suppresses the *Pnan* symmetry and creates polarity along the 2_1 axis parallel to **c** (Belokoneva *et al.*, 1997). However, some elements of the high-temperature structure are retained at room temperature in KTP and its isomorphs (Thomas *et al.*, 1990). As the temperature decreases from room temperature the K^+ cations move further away from the pseudosymmetric positions. Nevertheless, Thomas *et al.* (1992) reported the absence of a phase transition in KTP down to 90 K, and, in addition, Larsen (1995) studied the electron density distribution in KTP down to 9 K without detecting any phase transformations.

The electron density analysis in KTP conducted by Hansen *et al.* (1991) at room temperature indicated the presence of strong covalent bonds between Ti and O atoms. They pointed out that the nonlinear optical properties of KTP could be explained by the large hyperpolarizability of the short covalent Ti—O bonds, for which pronounced excess electron density was

ISSN 0108-7681

Table 1. *Experimental details*

	9.6 K	295 K
Crystal data		
Chemical formula	$RbTiOAsO_4$	$RbTiOAsO_4$
Chemical formula weight	288.27	288.27
Cell setting	Orthorhombic	Orthorhombic
Space group	$Pna2_1$	$Pna2_1$
a (Å)	13.218 (1)	13.261 (2)
b (Å)	6.6500 (9)	6.6791 (8)
c (Å)	10.761 (1)	10.769 (1)
V (Å^3)	945.89 (17)	953.8 (2)
Z	8	8
D_x (Mg m^{-3})	4.048	4.015
Radiation type	Mo $K\alpha$	Mo $K\alpha$
Wavelength (Å)	0.71069	0.71069
No. of reflections for cell parameters	20	18
θ range (°)	2.584–21.21	7.1–17.4
μ (mm^{-1})	18.9	18.74
Temperature (K)	9.6 (3)	295 (2)
Crystal form	KTP morphology	KTP morphology
Crystal size (mm)	0.58 × 0.54 × 0.36	0.58 × 0.54 × 0.36
Crystal colour	Colourless	Colourless
Data collection		
Diffractometer	Huber 512	Huber 512
Absorption correction	Analytical	Analytical
T_{min}	0.0078	0.0079
T_{max}	0.0660	0.0664
No. of measured reflections	15 878	9854
No. of independent reflections	5090	5125
No. of observed reflections	5020	4852
Criterion for observed reflections	$F > 2\sigma(F)$	$F > 2\sigma(F)$
R_{int}	0.022	0.055
θ_{max} (°)	50.13	50.08
Range of h, k, l	$-15 \rightarrow h \rightarrow 28$	$0 \rightarrow h \rightarrow 28$
	$-7 \rightarrow k \rightarrow 14$	$0 \rightarrow k \rightarrow 14$
	$-21 \rightarrow l \rightarrow 22$	$-21 \rightarrow l \rightarrow 22$
No. of standard reflections	3	3
Frequency of standard reflections	Every 100 reflections	Every 100 reflections
Refinement		
Refinement on	F	F
R	0.032	0.055
wR	0.026	0.042
S	4.56	4.845
No. of reflections used in refinement	5006	4796
No. of parameters used	146	146
Weighting scheme	$1/\sigma^2(F)$	$1/\sigma^2(F)$
$(\Delta/\sigma)_{max}$	0.3849×10^{-3}	0.2553×10^{-3}
$\Delta\rho_{max}$ (e Å^{-3})	1.53	3.06
$\Delta\rho_{min}$ (e Å^{-3})	−1.84	−2.84
Extinction method	Zachariasen (1968)	Zachariasen (1968)
Extinction coefficient	738 (9) × 10^1	1713 (24) × 10^1
Source of atomic scattering factors	*International Tables for X-ray Crystallography* (1974, Vol. IV, Tables 2.2B and 2.3.1)	*International Tables for X-ray Crystallography* (1974, Vol. IV, Tables 2.2B and 2.3.1)

observed. On the other hand, the earlier study of the electron distribution in KTP by Voloshina *et al.* (1985) indicated a high degree of polarization of the O atoms in the PO_4 tetrahedra. However, as Hansen *et al.* (1988) showed, the high nonlinear polarizability of KTP cannot be explained by the phosphate-group contribution alone. The electron density in KTP measured by Larsen (1995) at 9 K supported that conclusion.

As the spontaneous polarization in ferroelectric compounds results from a dipole-type polarization of the electron density in the unit cell, X-ray diffraction data collected at very low temperatures can give more accurate information on the electron density polarization, being less affected by harmonic and anharmonic thermal atomic displacements. Thus, the main purpose of the present study is to determine the structural and

electron-density changes in RTA by a single-crystal X-ray diffraction experiment at 9.6 K.

2. Experimental

RTA single crystals were grown by spontaneous crystallization from the $Rb_5As_3O_{10}$ self-flux, in which only constituents of the crystals are present, prepared from a powder mixture of Rb_2CO_3, TiO_2 and As_2O_5. A batch of approximately 0.5 g of RTA per 1 g of $Rb_5As_3O_{10}$ flux was mixed in a platinum crucible and inserted in a vertical tube furnace. The mixture was homogenized by stirring at 1270 K. Crystallization started at 1060 K with subsequent cooling at a rate of 2 K d^{-1}. The crystalline sample chosen for the X-ray diffraction experiments had a morphology typical of KTP with the dimensions given in Table 1. An as-grown crystal was used to avoid defects which are easily introduced in the material by cutting and polishing. The sample chosen was also larger than normally used for accurate single-crystal X-ray diffraction studies in order to increase the statistical precision of measured intensities, which is affected by the significant absorption of the incident beam by the Be windows in the cryostat tube. Crystal faces were measured and indexed using both scanning electron and optical microscopy.

Data were collected at 9.6 (3) K using a Displex 202D cryogenic refrigerator similar to that reported by Larsen (1995). Experimental details are given in Table 1. Three standard reflections, 800, 040 and 004, were used to monitor the experimental stability. The standards varied by less than 1%. An $\omega/2\theta$ scan mode was used to measure intensity profiles for a full sphere up to $2\theta = 50^\circ$ and then for a quarter of a sphere up to $2\theta = 100^\circ$. Fixed scan speeds of 3° min^{-1} for $2\theta = 2.5$–50° and 1.92° min^{-1} for $2\theta = 50$–100° were used. The intensities were calculated using the *PROFIT* profile-fitting program (Streltsov & Zavodnik, 1989). Before cooling the sample, a preliminary data measurement for a full sphere up to $2\theta = 50^\circ$ was conducted at room temperature. Then, after the low-temperature experiment and subsequent reheating, the same data set was recollected at room temperature, in order to detect any irreversible structural changes which might occur and remain in the crystal after reheating.

Integrated intensities were modified and structure-factor variances from counting statistics were adjusted for experimental instability as indicated by the standards (Rees, 1977). An analytical absorption correction (Alcock, 1974) was applied, which reduced the value of $R_{int}(F^2)$ from 0.030 to 0.022 for the low-temperature data. Lorentz and polarization corrections were applied. Further, symmetry-equivalent reflections were averaged. Variances consistent with measurement statistics were retained and those for the other measurements were increased according to the scatter of equivalents following a Fisher test (Hamilton, 1964).

Independent structural parameters, including the scale factor and positional and displacement parameters for all atoms, were refined by conventional full-matrix least squares including all observed structure factors. The independent atom model (IAM) was

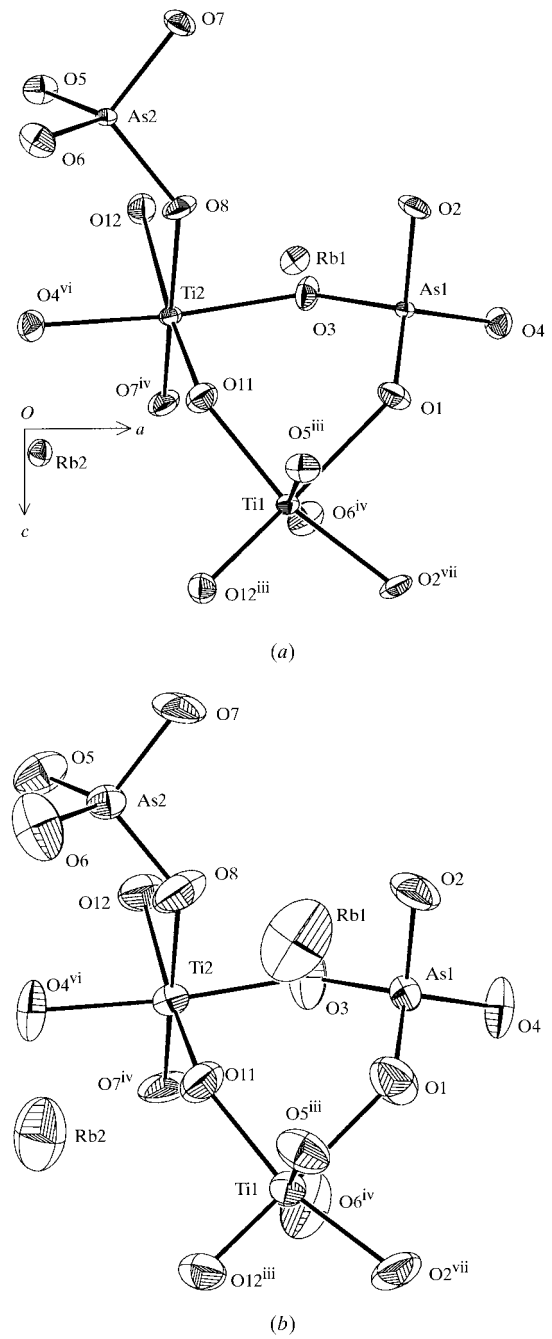

Fig. 1. *ORTEP* views of the structure at (*a*) low and (*b*) ambient temperatures projected onto the *ac* plane. Displacement ellipsoids are shown at the 99% probability level. Symmetry codes are given in Table 5.

Table 2. *Fractional atomic coordinates and equivalent isotropic (U_{eq}, Å^2) and anisotropic (U^{ij}, Å^2) displacement parameters at 9.6 K*

$$U_{\rm eq} = (1/3)\Sigma_i\Sigma_j U^{ij} a^i a^j \mathbf{a}_i.\mathbf{a}_j.$$

	x	y	z	$U_{\rm eq}$
Rb1	0.38187 (2)	0.78084 (4)	0.68708 (6)	0.00324 (11)
Rb2	0.10896 (2)	0.69237 (4)	0.93924 (6)	0.00295 (10)
Ti1	0.37402 (4)	0.50487 (9)	1.00918 (8)	0.00226 (17)
Ti2	0.24844 (4)	0.27027 (8)	0.75921 (8)	0.00213 (17)
As1	0.49955 (3)	0.32869 (4)	0.75244 (6)	0.00165 (10)
As2	0.18019 (2)	0.50527 (6)	0.49791 (6)	0.00173 (10)
O1	0.4880 (2)	0.4908 (4)	0.8669 (2)	0.0043 (9)
O2	0.5100 (2)	0.4617 (4)	0.6181 (2)	0.0040 (9)
O3	0.39501 (18)	0.1874 (4)	0.7305 (2)	0.0040 (8)
O4	0.59976 (18)	0.1752 (4)	0.7710 (2)	0.0042 (9)
O11	0.2820 (2)	0.4527 (4)	0.8681 (2)	0.0044 (9)
O12	0.2176 (2)	0.0556 (4)	0.6185 (2)	0.0041 (9)
O5	0.1098 (2)	0.3029 (4)	0.4616 (2)	0.0039 (9)
O6	0.1068 (2)	0.7045 (4)	0.5278 (2)	0.0047 (9)
O7	0.2588 (2)	0.5443 (4)	0.3744 (2)	0.0040 (9)
O8	0.2582 (2)	0.4585 (4)	0.6171 (8)	0.0042 (9)

	U^{11}	U^{22}	U^{33}	U^{12}	U^{13}	U^{23}
Rb1	0.00387 (10)	0.00235 (10)	0.00349 (12)	0.00030 (9)	−0.00057 (10)	−0.00031 (10)
Rb2	0.00258 (9)	0.00295 (9)	0.00331 (12)	0.00030 (9)	−0.00013 (10)	−0.00017 (10)
Ti1	0.00241 (14)	0.00253 (16)	0.0018 (2)	0.00007 (18)	−0.00010 (16)	−0.00025 (17)
Ti2	0.00236 (14)	0.00239 (17)	0.0016 (2)	−0.00005 (16)	−0.00020 (15)	0.00006 (17)
As1	0.00177 (9)	0.00188 (9)	0.00130 (11)	0.00003 (11)	0.00008 (9)	0.00011 (11)
As2	0.00210 (9)	0.00172 (10)	0.00136 (11)	−0.00005 (11)	0.00000 (11)	0.00018 (10)
O1	0.0047 (8)	0.0048 (9)	0.0033 (10)	−0.0015 (8)	0.0013 (7)	−0.0012 (8)
O2	0.0046 (9)	0.0051 (9)	0.0024 (10)	0.0009 (8)	0.0016 (7)	0.0009 (7)
O3	0.0025 (7)	0.0044 (8)	0.0052 (10)	−0.0009 (7)	−0.0006 (7)	0.0010 (8)
O4	0.0032 (8)	0.0047 (8)	0.0045 (11)	0.0011 (7)	−0.0001 (7)	−0.0007 (8)
O11	0.0044 (9)	0.0048 (9)	0.0040 (11)	0.0004 (8)	−0.0008 (7)	−0.0007 (8)
O12	0.0035 (8)	0.0046 (9)	0.0041 (11)	0.0001 (8)	−0.0002 (7)	−0.0012 (8)
O5	0.0053 (8)	0.0028 (8)	0.0037 (10)	−0.0012 (8)	−0.0002 (7)	−0.0002 (7)
O6	0.0057 (8)	0.0034 (8)	0.0052 (10)	0.0014 (8)	0.0013 (8)	−0.0002 (7)
O7	0.0043 (9)	0.0048 (9)	0.0030 (11)	0.0000 (8)	0.0012 (7)	0.0010 (8)
O8	0.0051 (9)	0.0050 (9)	0.0025 (10)	−0.0009 (8)	−0.0014 (7)	0.0013 (7)

used. Details of the data refinement are given in Table 1.† Zachariasen's extinction parameter r^* was refined in accordance with Larson's implementation (Larson, 1970). The minimum extinction-correction parameter $y_{\rm min}$ was 0.75 (0.63 at room temperature) for the 013 reflection (the observed structure factor $F_{\rm obs} = yF_{\rm kin}$, where $F_{\rm kin}$ is the kinematical value of the structure factor). The refined Flack (1983) parameter of 0.546 (6) [0.59 (1) at room temperature] shows that the crystal is nearly 50% of the [001] inversion twin. This is because the RTA crystal was grown spontaneously at a temperature close to T_c = 1073 K (Marnier *et al.*, 1989). All calculations were based on the *Xtal*3.4 system of crystallographic programs (Hall *et al.*, 1995) implemented on DEC-Alpha stations.

† Supplementary data for this paper are available from the IUCr electronic archives (Reference: OS0025). Services for accessing these data are described at the back of the journal.

3. Structural geometry

No phase transition was observed in the RTA structure between room temperature and 9.6 K. As expected, the unit-cell parameters and, consequently, the cell volume are reduced at 9.6 K compared with the room-temperature cell parameters in Table 1 and those reported by Thomas *et al.* (1992). The atomic coordinates and anisotropic displacement parameters are given in Table 2. For comparison, the room-temperature parameters measured in this study are given in Table 3. The coordinates are given in the same crystallographic setting used for $KSnOPO_4$ and $KTiOPO_4$ reported by Thomas *et al.* (1990), except for the z(Ti1) coordinate which has been transformed to connect the Ti1 atom to the other atoms in the asymmetric unit.

Although the observed changes in the Ti–O–As network are rather small as the temperature is lowered from 295 to 9.6 K, the Rb atoms move by about 0.04 (1) Å in the positive c direction further away from their pseudosymmetric positions in the room-

Table 3. *Fractional atomic coordinates and equivalent isotropic (U_{eq}, Å^2) and anisotropic (U^{ij}, Å^2) displacement parameters at 295 K*

$$U_{\rm eq} = (1/3)\Sigma_i\Sigma_j U^{ij} a^i a^j \mathbf{a}_i.\mathbf{a}_j.$$

	x	y	z	$U_{\rm eq}$
Rb1	0.38304 (6)	0.78228 (10)	0.68223 (13)	0.0209 (3)
Rb2	0.10905 (5)	0.69381 (11)	0.93537 (13)	0.0172 (3)
Ti1	0.37370 (7)	0.50486 (18)	1.00974 (15)	0.0060 (3)
Ti2	0.24874 (9)	0.26985 (15)	0.75971 (14)	0.0057 (3)
As1	0.49964 (5)	0.32826 (8)	0.75318 (12)	0.00538 (17)
As2	0.17988 (4)	0.50516 (11)	0.49892 (12)	0.00579 (18)
O1	0.4874 (4)	0.4888 (9)	0.8681 (5)	0.011 (2)
O2	0.5102 (4)	0.4614 (9)	0.6189 (5)	0.010 (2)
O3	0.3952 (4)	0.1881 (7)	0.7306 (5)	0.011 (2)
O4	0.6002 (3)	0.1776 (7)	0.7725 (5)	0.0095 (19)
O11	0.2818 (4)	0.4522 (8)	0.8683 (5)	0.009 (2)
O12	0.2177 (4)	0.0558 (8)	0.6181 (5)	0.009 (2)
O5	0.1099 (4)	0.3031 (7)	0.4607 (5)	0.0100 (18)
O6	0.1072 (4)	0.7043 (7)	0.5308 (5)	0.013 (2)
O7	0.2580 (4)	0.5444 (8)	0.3746 (4)	0.010 (2)
O8	0.2578 (4)	0.4584 (8)	0.6172 (15)	0.011 (2)

	U^{11}	U^{22}	U^{33}	U^{12}	U^{13}	U^{23}
Rb1	0.0226 (3)	0.0100 (3)	0.0299 (4)	0.0030 (3)	−0.0076 (3)	−0.0031 (3)
Rb2	0.0119 (2)	0.0155 (3)	0.0243 (4)	0.0035 (3)	−0.0013 (3)	−0.0020 (3)
Ti1	0.0059 (2)	0.0066 (3)	0.0054 (4)	0.0001 (4)	0.0002 (3)	−0.0008 (3)
Ti2	0.0059 (2)	0.0069 (3)	0.0044 (3)	−0.0002 (3)	−0.0005 (3)	−0.0001 (4)
As1	0.00448 (14)	0.00624 (16)	0.00542 (19)	−0.0000 (2)	0.00063 (16)	−0.0002 (2)
As2	0.00695 (16)	0.00517 (18)	0.0053 (2)	−0.0003 (2)	−0.0001 (2)	0.00068 (18)
O1	0.0104 (18)	0.013 (2)	0.010 (2)	−0.0024 (18)	0.0030 (15)	−0.0045 (18)
O2	0.011 (2)	0.014 (2)	0.0062 (19)	0.0028 (18)	0.0035 (15)	0.0042 (15)
O3	0.0061 (15)	0.0089 (17)	0.019 (3)	−0.0012 (16)	0.0000 (16)	−0.0002 (18)
O4	0.0038 (15)	0.0083 (16)	0.016 (3)	0.0008 (15)	−0.0011 (15)	0.0009 (17)
O11	0.0083 (18)	0.012 (2)	0.007 (2)	0.0010 (17)	−0.0025 (14)	−0.0019 (16)
O12	0.010 (2)	0.0106 (19)	0.006 (2)	0.0003 (17)	−0.0010 (14)	−0.0013 (15)
O5	0.0127 (18)	0.0085 (16)	0.009 (2)	−0.0023 (18)	−0.0034 (16)	−0.0005 (15)
O6	0.0116 (18)	0.0067 (16)	0.021 (3)	0.0029 (18)	0.0041 (18)	0.0015 (17)
O7	0.013 (2)	0.012 (2)	0.004 (2)	0.002 (2)	0.0022 (15)	0.0039 (15)
O8	0.013 (2)	0.014 (2)	0.008 (2)	−0.005 (2)	−0.0047 (16)	0.0027 (16)

temperature structure. *ORTEP* (Johnson *et al.*, 1972) plots of the RTA structure at 9.6 K and room temperature are given in Fig. 1. The equatorial planes of the Ti octahedra have been chosen to contain the central Ti atom and the two O atoms O11 and O12 that bind only to Ti atoms, creating periodic bond chains of markedly short and long bonds. This equatorial least-squares plane of the Ti1 octahedron is almost parallel to the *ac* or (010) plane with an angle between the planes of 10.45 (6)° at 9.6 K and 10.8 (1)° at 295 K. The atom-to-plane distances in Table 4 show that this plane is not the least distorted; the least distorted least-squares plane includes Ti1, O1, O5^{iii}, O6^{iv} and O12^{iii}. (Symmetry codes are given in Table 5.) In the equatorial plane, the *c* axis is approximately parallel to the O11–O12^{iii} vector and the *a* axis is approximately parallel to the O11–O1 vector. The O5^{iii} and O6^{iv} atoms are out of the plane and bonded to Ti1 along a line nearly parallel to the *b* axis. In the Ti2 octahedron, the equatorial plane is formed by O7^{iv}, O8, O11 and O12. It is almost parallel to the *bc* or (100) plane and the angles between the planes are 12.82 (6) and 12.7 (1)° at 9.6 and 295 K, respectively. The *c* axis is approximately parallel to the O8–O11 vector and the *b* axis is approximately parallel to the O7^{iv}–O11 vector. The apical O3 and O4^{vi} atoms are bonded to Ti2 along a line nearly parallel to the *a* axis. As indicated in Table 4, the atom-to-plane distances in the Ti octahedra do not change significantly with temperature. The only exception is the least-squares plane defined by Ti2, O3, O4^{vi}, O7^{iv} and O8, in which the atom-to-plane distances for O7^{iv} and O8 are significantly longer at 295 K than at 9.6 K.

A rigid-body analysis was performed using the *XP* program in the *SHELXTL-Plus* package (Sheldrick, 1990) to study possible collective translation, libration and screw (**TLS**) motions of atoms in the network structure. The **TLS** tensor elements are larger and the U^{ij}(obs) and U^{ij}(calc) values agree better for the As tetrahedra than for the Ti octahedra. The TiO_6 groups show less agreement with the rigid-body model. This is indicated by lower *R* factors of 0.078 for $As1O_4$ and 0.09 for $As2O_4$ compared with the *R* factors

Table 4. *Atom-to-plane distances (Å) to selected least-squares planes in the Ti octahedra*

Plane	9.6 K	295 K	Plane	9.6 K	295 K
Ti1	0.020 (1)	0.014 (2)	Ti2	0.015 (1)	0.009 (2)
O1	0.118 (3)	0.126 (7)	O7^{iv}	0.010 (4)	0.013 (8)
O2^{vii}	0.056 (3)	0.050 (7)	O8	0.076 (9)	0.08 (2)
O11	0.054 (3)	0.044 (7)	O11	0.049 (3)	0.052 (7)
O12^{iii}	0.137 (3)	0.134 (7)	O12	0.040 (3)	0.042 (7)
Ti1	0.010 (1)	0.007 (2)	Ti2	0.029 (1)	0.021 (1)
O1	0.018 (3)	0.019 (7)	O3	0.096 (3)	0.104 (7)
O5^{iii}	0.044 (3)	0.050 (7)	O4^{vi}	0.106 (3)	0.112 (7)
O6^{iv}	0.049 (3)	0.057 (7)	O7^{iv}	0.001 (4)	0.036 (8)
O12^{iii}	0.007 (3)	0.005 (7)	O8	0.001 (8)	0.29 (2)

Symmetry codes are given in Table 5.

of 0.146 and 0.116 for the Ti1 and Ti2 octahedra, respectively. However, the *R* factors increase significantly for the $As2O_4$ tetrahedron at 9.6 K, suggesting that the rigid-body model is less relevant at low temperatures.

Selected bond distances (uncorrected for libration) and angles are given in Table 5. No significant changes were noted in the bond lengths between the Ti, O11 and O12 atoms. The Ti1—O5^{iii} and Ti1—O6^{iv} bond distances and the Ti2—O4^{vi}—As1^{vi} and O3—As1—O4 angles decrease slightly with temperature. Concurrently, the O5—As2—O7 angle shows a small increase. Both Rb1 and Rb2 are located in channels along the *c* axis and are coordinated by nine O atoms. The Rb—O bonds are longer in the positive than in the negative *c* direction. As the Rb atoms move along the positive *c* direction with decreasing temperature, the bond distances in this direction become shorter and the bond angles increase. However, the Rb1—O6^{ii} bond vector directed parallel to the negative *c* axis significantly increases while the temperature decreases from 295 to 9.6 K. Table 6 gives the displacement parameters along the principal axes, calculated using the *ORFFE* program modified for a PC (Busing *et al.*, 1964; Gustafsson, 1993). The Rb1 atom vibrates predominantly in the [$\bar{1}$01] direction, while the Rb2 atom vibrates strongly in the [001] direction. The O atoms show pronounced anisotropic displacements at room temperature. The O3 and O4 atoms, which link together the Ti2 octahedra and the As1 tetrahedra forming periodic bond chains along the *a* axis, have larger displacements in the [001] direction. The O6 atomic displacement parameter along the polar *c* axis is also significantly larger than in other directions.

4. Electron density

Atomic charges were estimated from the difference electron density ($\Delta\rho = \rho_{exp} - \rho_{IAM}$) using Hirshfeld partitioning (Hirshfeld, 1977). The signs of the charges are in accordance with the atomic electronegativities. The average charges for the Ti and As atoms are estimated to be +0.5 (5) e and the average charge for the O atoms is approximately −0.3 (3) e, which is similar to that for the O atoms in $LiNbO_3$ estimated by the same procedure (Hsu *et al.*, 1997). For Rb the average charge is estimated to be approximately +0.6 (4) e.

In order to identify qualitatively the features of the charge distribution common to RTA and other members of the KTP family, the calculation of difference electron density ($\Delta\rho$) maps was attempted. Fig. 2 shows $\Delta\rho$ maps in different planes for RTA at 9.6 K. The contour interval is 0.4 e Å^{-3}, whereas the mean standard uncertainty is 0.25 e Å^{-3}. Fig. 2(*a*) depicts the $\Delta\rho$ in the near equatorial (010) plane through Ti1. The $\Delta\rho$ map in the least-squares plane defined by Ti1 and four O atoms and the map in the plane through Ti1 and two O atoms show similar topologies. This is because the atoms do not deviate significantly from the (010) plane. There is significant density concentration at a distance of 0.5 Å from Ti1 near the shortest Ti1—O12^{iii} bond of 1.722 (3) Å. The excess $\Delta\rho$ is shifted towards Ti1 in the −**c** direction away from the Ti—O12 line. The Ti1 nucleus is on a slope of the $\Delta\rho$ function with the excess electron density along −**c** and the electron-density depletion along +**c**. The $\Delta\rho$ near the Ti1 atom in the plane perpendicular to the equatorial plane does not show such strong dipole-like asymmetry. The $\Delta\rho$ map in the (100) plane through the Ti2 atom is shown in Fig. 2(*b*). In the Ti2 octahedron, all equatorial atoms are close to the (100) plane through Ti2. The electron density near Ti2 is polarized along −**c**, similar to that for Ti1 in Fig. 2(*a*). In general these features are close to those observed in KTP by Hansen *et al.* (1991) at room temperature and by Larsen (1995) at 9 K. These reproducible features of the $\Delta\rho$ distribution in the KTP family of compounds improve our confidence in the results obtained, even though a large crystal sample had to be used for the 9.6 K experiment.

Fig. 2(*c*) shows the $\Delta\rho$ map in the (010) plane through Rb1. The electron density near Rb1 is polarized in the +**c** direction and a dipole-like deformation is stretched along the polar **c** direction. The *bc* plane shows the same dipole-like feature around the Rb1 atom in the **c** direction. The $\Delta\rho$ maps in the same planes through Rb2

Table 5. *Selected geometric parameters (Å, °)*

	9.6 K	295 K
Rb1—O1	3.071 (3)	3.125 (6)
Rb1—O11	3.209 (3)	3.268 (5)
Rb1—O12	2.932 (3)	2.937 (6)
Rb1—O6^{ii}	3.434 (3)	3.392 (6)
Rb2—O11	2.891 (3)	2.893 (5)
Rb2—O12^{iii}	3.131 (3)	3.163 (5)
Rb2—O2^{iii}	3.063 (3)	3.099 (6)
Ti1—O1	2.150 (3)	2.147 (6)
Ti1—O11	1.977 (3)	1.982 (5)
Ti1—O2^{vii}	1.942 (3)	1.950 (5)
Ti1—O5^{iii}	2.058 (3)	2.072 (5)
Ti1—O6^{iv}	2.023 (3)	2.036 (5)
Ti1—O12^{iii}	1.722 (3)	1.716 (5)
Ti2—O3	2.038 (2)	2.042 (5)
Ti2—O12	2.121 (3)	2.131 (5)
Ti2—O7^{iv}	1.950 (3)	1.950 (5)
Ti2—O4^{vi}	2.002 (2)	2.005 (5)
Ti2—O11	1.744 (3)	1.745 (5)
Ti2—O8	1.980 (7)	1.989 (13)
As1—O1	1.644 (3)	1.646 (6)
As1—O2	1.701 (3)	1.703 (5)
As1—O3	1.688 (2)	1.689 (5)
As1—O4	1.684 (2)	1.684 (5)
As2—O5	1.682 (3)	1.689 (5)
As2—O7	1.706 (3)	1.713 (5)
As2—O6	1.673 (3)	1.678 (5)
As2—O8	1.675 (6)	1.669 (13)
O1—Rb1—O11	51.58 (7)	50.65 (14)
O1—Rb1—O12^{i}	152.65 (7)	150.65 (15)
O11—Rb1—O12^{i}	105.77 (7)	104.90 (14)
O11—Rb2—O12^{iii}	54.82 (7)	54.37 (14)
O11—Rb2—O2^{iii}	153.49 (7)	152.23 (15)
O12^{iii}—Rb2—O2^{iii}	99.13 (7)	98.17 (14)
O3—As1—O4	108.85 (12)	109.6 (2)
O5—As2—O7	106.09 (13)	105.3 (3)
Ti2—O4^{vi}—As1^{vi}	130.89 (14)	131.7 (3)

Symmetry codes: (i) $x, 1+y, z$; (ii) $\frac{1}{2}+x, \frac{3}{2}-y, z$; (iii) $\frac{1}{2}-x, \frac{1}{2}+y, \frac{1}{2}+z$; (iv) $\frac{1}{2}-x, y-\frac{1}{2}, \frac{1}{2}+z$; (v) $x-\frac{1}{2}, \frac{3}{2}-y, z$; (vi) $x-\frac{1}{2}, \frac{1}{2}-y, z$; (vii) $1-x, 1-y, \frac{1}{2}+z$.

Table 6. *Thermal displacements (Å) along principal axes and angles (°) between the principal axes and the c axis of the unit cell*

		9.6 K	Angle	295 K	Angle
Rb1	r_1	0.047 (1)	81 (6)	0.096 (2)	85 (1)
	r_2	0.056 (1)	143 (4)	0.134 (1)	123.5 (9)
	r_3	0.0663 (8)	126 (3)	0.188 (1)	33.9 (8)
Rb2	r_1	0.049 (1)	93 (6)	0.099 (2)	90 (1)
	r_2	0.055 (1)	125 (10)	0.130 (1)	108 (2)
	r_3	0.059 (1)	35 (10)	0.158 (1)	18 (2)
O3	r_1	0.045 (9)	85 (17)	0.07 (1)	97 (11)
	r_2	0.062 (8)	131 (18)	0.09 (1)	103 (11)
	r_3	0.077 (7)	41 (18)	0.14 (1)	14 (10)
O4	r_1	0.051 (9)	99 (19)	0.061 (9)	84 (9)
	r_2	0.067 (8)	141 (26)	0.09 (1)	85 (14)
	r_3	0.077 (7)	53 (26)	0.13 (1)	8 (12)
O6	r_1	0.05 (1)	109 (16)	0.07 (2)	90 (90)
	r_2	0.068 (7)	142 (18)	0.11 (1)	67 (10)
	r_3	0.083 (6)	59 (16)	0.15 (1)	23 (10)

show similar topologies with the $\Delta\rho$ dipoles near Rb2 aligned along **c**. The peaks near Rb atoms could be an indication of split positions (Thomas & Womersley, 1998). However, refinements did not give any significant population of the shifted sites. Fig. 2(*d*) depicts the $\Delta\rho$ in the plane approximately parallel to the *ab* plane through the As1—O3 and As1—O4 bonds. The electron density accumulates in the areas between the As1 and O atoms, and can be attributed to the covalent bonding. However, these excess densities are shifted away from the interatomic lines and are located approximately on the line parallel to the *a* axis though As1. The $\Delta\rho$ maps in the As1 and As2 tetrahedra show similar features. Near the As atoms, the $\Delta\rho$ is not polarized in the same way as near the Ti and Rb atoms, and the As—O bonds appear to be bent with the electron density shifted away from the bond directions. The As—O bonds in RTA exhibit different $\Delta\rho$ features compared with those of the phosphate groups in KTP (Hansen *et al.*, 1991) and in $LiFePO_4$ (Streltsov *et al.*, 1993).

The electron density maps at room temperature show, in general, main features close to those obtained at low temperature. More accurate measurements of the electron density at room temperature using high-flux synchrotron radiation will be presented elsewhere.

5. Discussion

Even though there is no phase transition in RTA from room temperature to 9.6 K and the structural network does not change to a notable extent, the Rb atoms move about 0.04 (1) Å in the network channels in the positive *c* direction. However, these shifts of the Rb atoms are still significantly smaller than the calculated phase-transition shifts of 0.54 (1) and 0.58 (1) Å for a temperature change from above T_c to 295 and 9.6 K, respectively. In turn, the phase-transition shifts of the Rb atoms are slightly smaller than Δz(K) of about 0.6 Å for KTP estimated by Thomas *et al.* (1990). The difference in the Rb and K shifts correlates with the difference in T_c values for RTA and KTP in accordance with the Abrahams–Jamieson–Kurtz criteria (Abrahams, 1994). Similarly, Belokoneva *et al.* (1997) have shown that the Δz shifts increase with T_c in a series of germanate analogues of KTP.

At 9.6 K all atoms show approximately the same slightly anisotropic thermal vibrations, but, as the temperature increases, the atomic displacements of Rb1 and Rb2 become far more pronounced than those for the other atoms. The large atomic displacements at room temperature indicate that the Rb atoms are less strongly bound and can be shifted to equivalent centrosymmetrical positions at temperatures $T > T_c$. Both Rb1 and Rb2 oscillate predominantly in the **c** direction. Some O atoms also have anisotropic displacement parameters

that are larger along **c** than along the **a** or **b** directions. The Rb1—O6^{ii} bond is the longest in the RTA structure and the O6 vibrations are pronounced in the **c** direction. At 9.6 K, the equivalent isotropic displacement parameter for O6 is significantly larger than those of the other atoms. In the room-temperature structure, O6 also has a slightly larger isotropic displacement parameter than the other atoms with the exception of Rb. The other atoms with predominant displacements along the *c* axis are O3 and O4. The Rb1—O3^{i} bond length is the shortest among the Rb1—O bonds at both temperatures. While O4 does not coordinate to Rb1, both O3^{iii} and O4^{vi} form intermediate-length bonds with the Rb2 atom.

The electron density distribution in the RTA structure at low temperature shows asymmetrical dipole-like features near the Ti and Rb sites aligned in the *c* direction. As spontaneous polarization in ferroelectric compounds results from shifts of electron density, this suggests that the Ti and Rb atoms are mainly responsible for the ferroelectricity of RTA. The As atoms do not show dipole-character deformations. The asym-

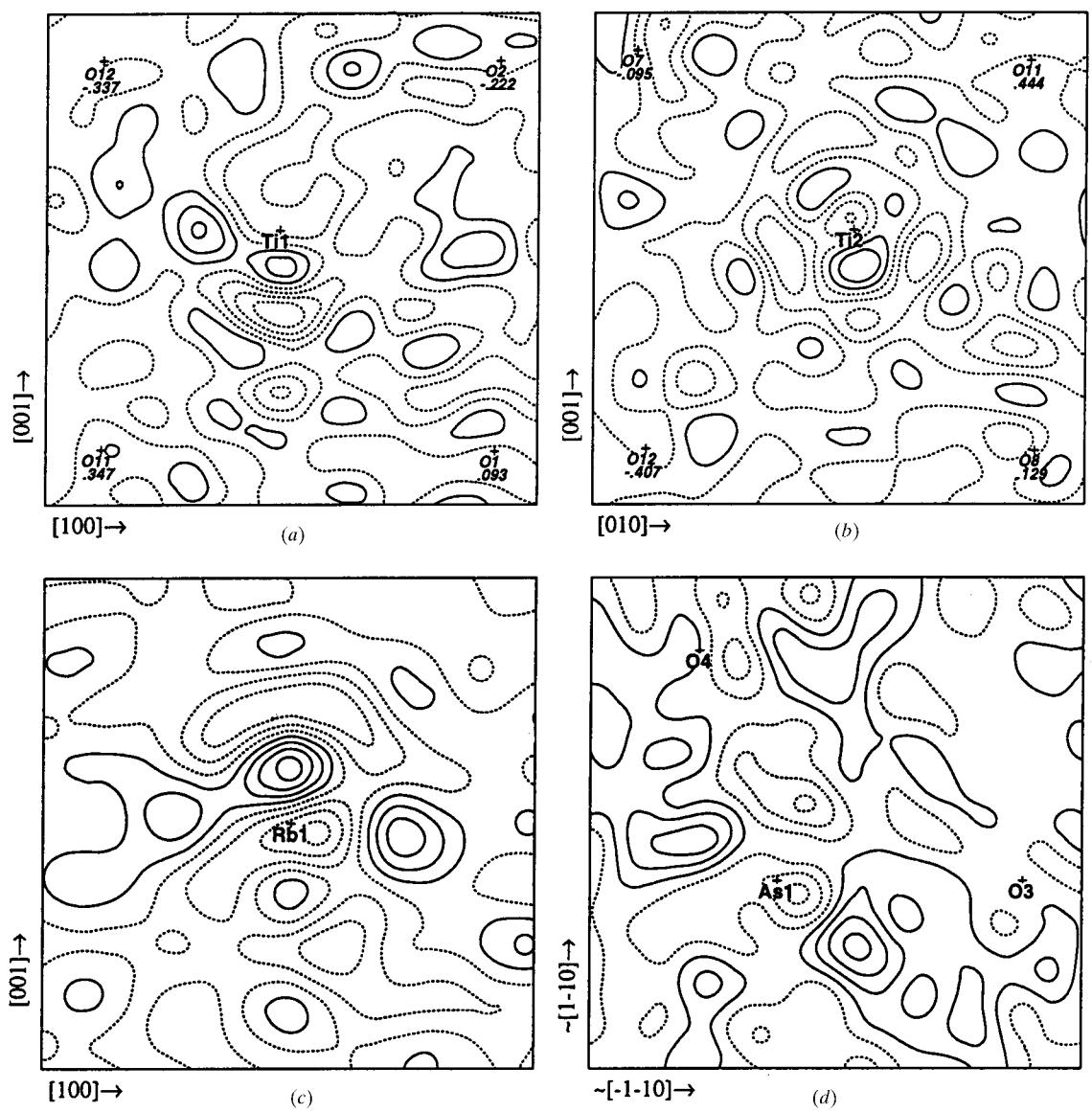

Fig. 2. $\Delta\rho$ maps drawn with positive contours as solid lines, negative contours as dashed lines and an increment interval of 0.4 e Å^{-3} [$\sigma(\Delta\rho)$ = 0.25 e Å^{-3}] for (*a*) the (010) plane through Ti1, (*b*) the (100) plane through Ti2, (*c*) the (010) plane through Rb1 and (*d*) the plane through As1, O3 and O4. The borders are 3.5 Å for (*a*), (*b*) and (*d*), and 2.5 Å for (*c*).

metric $\Delta\rho$ features appear in the equatorial planes defined by the Ti, O11 and O12 atoms. The electron density within the Ti octahedra accumulates predominantly in the exceptionally short Ti1—$O12^{iii}$ and Ti2—O11 bonds. Strong accumulation and polarization of the electron density in the short covalent Ti—O bonds alternates with the depleted density in the long Ti—O bonds in RTA. This suggests possible delocalization of the electron density and charge transfer along these periodic bonding chains, which is favourable for the nonlinear optical properties of RTA.

This work was supported by the Swedish Natural Science Research Council (NFR) and the Chalmers Foundation. JA and JA wish to express their gratitude to the University of Western Australia Crystallography Centre and Chemistry Department for their kind hospitality.

References

Abrahams, S. C. (1994). *Acta Cryst.* A**50**, 658–685.
Alcock, N. W. (1974). *Acta Cryst.* A**30**, 332–335.
Belokoneva, E. L., Dolgushin, F. M., Antipin, M. Yu., Mill, B. V. & Struchkov, Yu. T. (1993). *Russ. J. Inorg. Chem.* **38**, 584–588.
Belokoneva, E. L., Knight, K. S., David, W. I. F. & Mill, B. V. (1997). *J. Phys. Condens. Matter*, **9**, 3833–3851.
Busing, W. R., Martin, K. O. & Levy, H. A. (1964). *ORFFE.* Report ORNL-TM-306. Oak Ridge National Laboratory, Tennessee, USA.
Flack, H. D. (1983). *Acta Cryst.* A**39**, 876–881.
Gustafsson, T. (1993). *ORFFE for PC/VAX.* Personal communication.
Hall, S. R., King, G. S. D. & Stewart, J. M. (1995). Editors. *Xtal3.4 User's Manual.* Perth: Lamb.
Hamilton, W. C. (1964). *Statistics in Physical Science.* New York: Ronald Press.
Hansen, N. K., Protas, J. & Marnier, G. (1988). *C. R. Acad. Sci. Ser. B*, **307**, 475–478.
Hansen, N. K., Protas, J. & Marnier, G. (1991). *Acta Cryst.* B**47**, 660–672.
Harrison, W. T. A., Gier, T. E., Stucky, G. D. & Schultz, A. J. (1990). *J. Chem. Soc. Chem. Commun.* pp. 540–542.
Hirshfeld, F. (1977). *Isr. J. Chem.* **16**, 198–201.
Hsu, R., Maslen, E. N., du Boulay, D. & Ishizawa, N. (1997). *Acta Cryst.* B**53**, 420–428.
Hu, Z. W., Thomas, P. A., Webjörn, J. & Loiacono, G. M. (1996). *J. Phys. D Appl. Phys.* **29**, 1681–1684.
Johnson, C. K., Guerdon, J. F., Richard, P., Whitlow, S. & Hall, S. R. (1972). *ORTEP. The XRAY System of Crystallographic Programs.* Technical Report TR-192. Computer Science Center, University of Maryland, College Park, Maryland, USA.
Karlsson, H., Laurell, F., Henriksson, P. & Arvidsson, G. (1996). *Electron. Lett.* **32**, 556–557.
Larsen, F. K. (1995). *Acta Cryst.* B**51**, 468–482.
Larson, A. C. (1970). *Crystallographic Computing*, edited by F. R. Ahmed, S. R. Hall & C. P. Huber, pp. 291–294. Copenhagen: Munksgaard.
Mangin, J., Marnier, G., Boulanger, B. & Menaert, B. (1989). *Inst. Phys. Conf. Ser.* No. 103, Part 1, pp. 65–68.
Marnier, G., Boulanger, B. & Menaert, B. (1989). *J. Phys. Condens. Matter*, **1**, 5509–5513.
Rees, B. (1977). *Isr. J. Chem.* **16**, 180–186.
Risk, W. P. & Loiacono, G. M. (1996). *Appl. Phys. Lett.* **69,** 311–313.
Sheldrick, G. M. (1990). *SHELXTL-Plus. Structure Determination Software Programs.* Siemens Analytical X-ray Instruments Inc., Madison, Wisconsin, USA.
Stefanovich, S., Musonov, A., Mill, B. & Belokoneva, E. (1996). *Ferroelectrics*, **185**, 63–66.
Streltsov, V. A., Belokoneva, E. L., Tsirelson, V. G. & Hansen, N. K. (1993). *Acta Cryst.* B**49**, 147–153.
Streltsov, V. A. & Zavodnik, V. E. (1989). *Sov. Phys. Crystallogr.* **34**, 824–828.
Stucky, G. D., Phillips, M. L. F. & Gier, T. E. (1989). *Chem. Mater.* **1**, 492–509.
Thomas, P. A., Glazer, A. M. & Watts, B. E. (1990). *Acta Cryst.* B**46**, 333–343.
Thomas, P. A., Mayo, S. C. & Watts, B. E. (1992). *Acta Cryst.* B**48**, 401–407.
Thomas, P. A. & Womersley, M. N. (1998). *Acta Cryst.* B**54**, 645–651.
Tordjman, I., Masse, R. & Guitel, J. C. (1974). *Z. Kristallogr.* **139**, 103–115.
Voloshina, L. V., Gerr, R. G., Antipin, M. Yu., Tsirelson, V. G., Pavlova, N. I., Struchkov, Yu. T., Ozerov, R. P. & Rez, I. S. (1985). *Sov. Phys. Crystallogr.* **30**, 389–393.
Zachariasen, W. H. (1968). *Acta Cryst.* A**24**, 212–216.